Journal of Materials Chemistry A

Accepted Manuscript

ROYAL SOCIETY OF CHEMISTRY

www.rsc.org/materialsA

Journal of Materials Chemistry A

ARTICLE

Energy Level Engineering of Thieno[3,4-*b*]pyrazine based Organic Sensitizers for Quasi-Solid-State Dye-Sensitized Solar Cells

Received 00th January 20xx,
Accepted 00th January 20xx

DOI: 10.1039/x0xx00000x

www.rsc.org/

Jinhong Wu, Guangfeng Li, Lu Zhang, Gang Zhou,* and Zhong-Sheng Wang

Thieno[3,4-*b*]pyrazine based organic sensitizers with cyanoacrylic acid (**FNE64** and **FNE66**) or carboxylic acid (**FNE65** and **FNE67**) as anchoring group have been designed and synthesized to optimize the lowest unoccupied molecular orbital (LUMO) level of panchromatic sensitizer **FNE32** with identical auxiliary electron acceptor. Their absorption, electrochemical and photovoltaic properties are systematically investigated. It is found that sensitizers **FNE65** and **FNE67** with carboxylic acid as anchoring group possess more negative LUMO levels as compared with sensitizers **FNE64** and **FNE66** with cyanoacrylic acid as anchoring group. In addition to tuning the LUMO level of thieno[3,4-*b*]pyrazine based organic sensitizer **FNE32** by attaching different anchoring group, the number of the bridged benzene ring has been optimized and two types organic sensitizers with D-A-π-A (**FNE64** and **FNE65**) and D-π-A-π-A (**FNE66** and **FNE67**) frameworks have been comparatively investigated. Upon the incorporation of an additional phenylene unit into sensitizers **FNE64** and **FNE65** with D-A-π-A configuration, sensitizers **FNE66** and **FNE67** with D-π-A-π-A structure exhibit unusual hypsochromically shifted absorption maxima. Moreover, the LUMO levels of the thieno[3,4-*b*]pyrazine based sensitizers **FNE66** and **FNE67** are lifted up, which results in a dramatically improved driving force for the electron injection from the excited dye molecules to the conduction band of the titania semiconductor. Consequently, the power conversion efficiency of the quasi-solid-state dye-sensitized solar cell (DSSC) based on **FNE66** increases by 95% in comparison to that for the quasi-solid-state DSSC based on panchromatic sensitizer **FNE32** whose photo-response range is over 900 nm. Our findings will facilitate the understanding of the crucial importance of energy level engineering and presents a way for tuning the LUMO levels of organic sensitizers at a fixed electron acceptor.

Introduction

Since the pioneering work of O'Regan and Grätzel in 1991,[1] dye-sensitized solar cells (DSSCs) have been investigated extensively as potential candidates for renewable energy system. The past decade has witnessed a steady increase of power conversion efficiency (η) for metal sensitizer based DSSCs.[2] Among these sensitizers, zinc porphyrin sensitizer SM315 has reaped a η record of 13% without the assistance of any co-sensitizer.[3] Concerning the cost and environment issues of metal-based sensitizers, many research groups have focused on metal-free organic sensitizers owing to their unique advantages, such as high molar extinction coefficients, low synthetic and purification cost, tunable photophysical properties via molecular engineering, and essentially no resource limitation.[4] Nevertheless, despite these attractions, the performance of DSSCs based on metal-free organic dyes has lagged behind those traditional metal–based organic dyes.[5] Encouragingly, pure organic dye based DSSC has recently achieved an efficiency of 12.5%[6] under the illumination of simulated AM1.5G solar light at one sun. However, most highly efficient DSSCs have been realized employing volatile organic liquid electrolytes which have suffered from the leakage problems and limit their outdoor applications. Alternatively, non-volatile ionic liquid or non-flowing (quasi-)solid-state electrolyte have been utilized in DSSCs to overcome such shortcoming.[7] Although significantly improved long-term stability has been achieved for these DSSCs based on non-liquid electrolyte, highly efficient and stable DSSCs are still pursed for their outdoor applications.

In a typical DSSC, the photocurrent is basically determined by the light harvesting efficiency of the dye molecules. Therefore, great efforts have focused on developing novel organic sensitizers with reduced energy gap by either raising the highest occupied molecular orbital (HOMO) or lowering the lowest unoccupied molecular orbital (LUMO) of the organic sensitizer, or both.[8] Meanwhile, suitable HOMO and LUMO energy levels of the sensitizer are required to match the iodide/triiodide redox potential and the conduction band edge of the TiO_2 semiconductor to ensure efficient dye regeneration and electron injection from the excited dye molecules into the TiO_2 conduction band. Consequently, a balance between wide absorption spectrum and suitable energy level is of great importance to construct ideal sensitizers for DSSCs.

Thieno[3,4-*b*]pyrazine, a strong electron-deficient group, has been extensively studied as a unique electron acceptor

Lab of Advanced Materials & Department of Chemistry, Collaborative Innovation Center of Chemistry for Energy Materials, Fudan University, Shanghai 200438, P. R. China. E-mail: zhougang@fudan.edu.cn.

and engaged into donor-acceptor low band gap polymers for organic photovoltaics (OPVs).[9] Recently, we have incorporated thieno[3,4-*b*]pyrazine as auxiliary acceptor group into D-π-A featured organic sensitizers and constructed panchromatic sensitizer **FNE32**[10] (**Fig. 1**) whose maximum absorption band located at around 600 nm. However, although the corresponding DSSC exhibited very broad IPCE spectra over the whole visible range extending into the near infrared (NIR) region up to 900 nm, the η value was limited to only 3.7% due to the insufficient driving force for the electron injection from the excited organic dyes into the TiO_2 film. Therefore, further molecular optimization is needed to tune the energy levels of the organic sensitizers for improving the DSSC performance.

In D-π-A-π-A featured organic sensitizers, it has been well established that the LUMO levels can be finely tuned by structural modification of the inserted auxiliary acceptor A'.[11] However, few work has been carried out to optimize the LUMO levels by adjusting other building blocks in D-π-A-π-A framework at a fixed A'.[12] Herein, the π-conjugated spacers and the anchoring groups are adjusted to lift up the LUMO levels of thieno[3,4-*b*]pyrazine based organic sensitizer. The bridged thiophene ring in sensitizer **FNE32** is replaced by benzene ring and two types organic sensitizers with D-A-π-A (**FNE64** and **FNE65**) and D-π-A-π-A (**FNE66** and **FNE67**) frameworks have been constructed, as shown in **Fig. 1**. Although incorporation of benzene ring[13] can generally extend the π-conjugation and bathochromically shift the maximum absorption wavelength of organic semiconductor, it is found that D-π-A-π-A configuration is superior to D-A-π-A configuration in increasing the energy band gap and lifting up the LUMO levels. Moreover, a much weaker electron withdrawing group, carboxylic acid, is introduced as anchoring group instead of the traditional cyanoacrylic acid group, which successfully raise the LUMO levels and enhancing the electron injection driving force in the related DSSCs. As a result, the η value of the quasi-solid-state DSSC based on **FNE66** increases by 95% in comparison to that for the quasi-solid-state DSSC based on **FNE32** with the same electron acceptor.

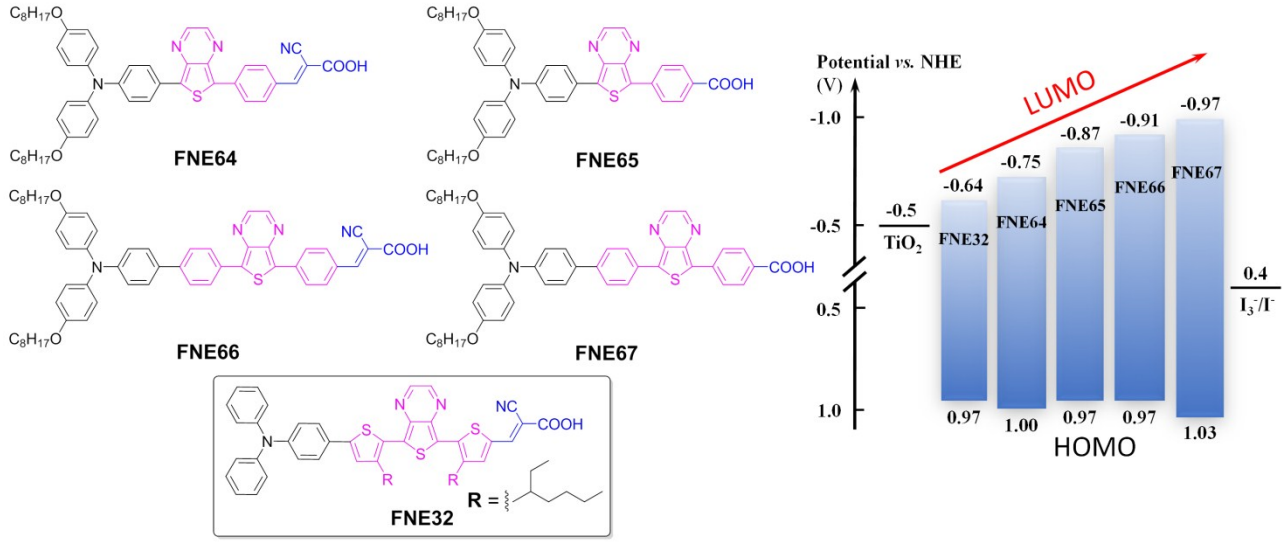

Fig. 1. Chemical structures and energy level diagrams of sensitizers **FNE64**-**FNE67** and reference **FNE32**.

Experimental Section

Materials and Reagents.

4-Formylbenzeneboronic acid and 4-methoxycarbonyl-benzeneboronic acid were purchased from J&K Chemical, Ltd. Organic solvents were purified using standard process. Anhydrous tetrahydronfuran (THF) was distilled from sodium benzophenone ketyl. DCM and *N*,*N*-Dimethylformamide (DMF) were distilled from CaH_2. Other chemicals and reagents were used as received from commercial sources without further purification. All reactions and manipulations were carried out under nitrogen with the use of standard inert atmosphere and Schlenk techniques. 2,5-Dibromothieno[3,4-*b*]pyrazine (**1**) were synthesized according to previously reported literature.[14] Transparent conductive glass (F-doped SnO_2, FTO, 14 Ω per square, transmittance of 85%, Nippon Sheet Glass Co., Japan) was used as the substrate for the fabrication of DSSC.

Synthesis of 4-(7-bromothieno[3,4-*b*]pyrazin-5-yl)benzaldehyde (3a)

Under a nitrogen atmosphere, a mixture of 2,5-dibromothieno[3,4-*b*]pyrazine (**1**)[14] (300 mg, 1.02 mmol), 4-formylbenzeneboronic acid (**2a**) (153 mg, 1.02 mmol), $Pd(PPh_3)_4$ (59 mg, 0.05 mmol) and K_2CO_3 (1.38 g, 0.01 mol) in a mixed solution of THF (15 mL), toluene (15 mL), and water (5 mL) was stirred and heated at 85 °C for 15 h. When the reaction was completed, the mixture was extracted with CH_2Cl_2 for three times. The combined organic solution was washed with brine and dried with anhydrous sodium sulfate. The solvent was removed with a rotary evaporator, and the residue was purified on a silica gel column with DCM/PE (1/1, v/v) as eluent. Orange solid **3a** was obtained with a yield 40% (130 mg). ^{1}H NMR (400 MHz, $CDCl_3$, δ ppm): 10.04 (s, 1H), 8.60

(d, 1H, *J* = 1.2 Hz), 8.57 (d, 1H, *J* = 1.2 Hz), 8.27 (d, 2H, *J* = 8.2 Hz), 7.96 (d, 2H, *J* = 8.1 Hz). ^{13}C NMR (100 MHz, $CDCl_3$, *δ* ppm): 191.7, 145.9, 145.3, 139.7, 138.3, 135.6, 130.6, 128.3, 109.7, 107.8. HRMS: m/z calcd for $C_{13}H_7BrN_2OS$, 317.9462; found 317.9453.

Synthesis of methyl 4-(7-bromothieno[3,4-*b*]pyrazin-5-yl)benzoate (3b)

Compound **3b** was synthesized via Suzuki coupling between compound **1** and 4-methoxycarbonylbenzeneboronic acid (**2b**) similarly as described for compound **3a**. Orange solid, yield 30% (142 mg). ^{1}H NMR (400 MHz, $CDCl_3$, *δ* ppm): 8.58 (d, 1H, *J* = 1.2 Hz), 8.56 (d, 1H, *J* = 1.2 Hz), 8.15 (q, 4H), 3.95 (s, 3H). ^{13}C NMR (100 MHz, $CDCl_3$, *δ* ppm): 166.9, 145.1, 142.2, 139.4, 136.8, 130.5, 129.7, 127.8, 106.9, 52.5. HRMS: m/z calcd for $C_{14}H_9BrN_2O_2S$, 347.9568; found 347.9541.

Synthesis of 4-(7-(4-(bis(4-(octyloxy)phenyl)amino)phenyl)thieno[3,4-*b*]pyrazin-5-yl)benzaldehyde (4a)

Compound **4a** was synthesized via Suzuki coupling between compound **3a** and *N*,*N*-bis[4-(octyloxy)phenyl]-4-(4,4,5,5-tetramethyl-1,3,2-dioxaborolan-2-yl)aniline similarly as described for compound **3a**. Blue solid, yield 75% (114 mg). ^{1}H NMR (400 MHz, $CDCl_3$, *δ* ppm): 10.00 (s, 1H), 8.53 (s, 1H), 8.48 (s, 1H), 8.36 (d, 2H, *J* = 8.3 Hz), 7.95 (d, 2H, *J* = 3.8 Hz), 7.92 (d, 2H, *J* = 3.3 Hz), 7.10 (d, 4H, *J* = 8.80 Hz), 6.98 (d, 2H, *J* = 8.8 Hz), 6.84 (d, 4H, *J* = 8.8 Hz), 3.94 (t, 4H, *J* = 6.5 Hz), 1.78-1.82 (m, 4H), 1.20-1.42 (m, 20H), 0.89 (t, 6H, *J* = 6.5 Hz). ^{13}C NMR (100 MHz, $CDCl_3$, *δ* ppm): 191.8, 156.2, 149.6, 144.9, 143.8, 141.8, 140.1, 139.9, 134.8, 130.5, 129.2, 127.8, 127.4, 124.1, 119.1, 115.6, 68.5, 32.0, 29.9, 29.6, 29.5, 26.3, 22.9, 14.3. HRMS: m/z calcd for $C_{47}H_{53}N_3O_3S$, 739.3808; found 739.3807.

Synthesis of methyl 4-(7-(4-(bis(4-(octyloxy)phenyl)amino)phenyl)thieno[3,4-*b*]pyrazin-5-yl)benzoate (4b)

Compound **4b** was synthesized via Suzuki coupling between compound **3b** and *N*,*N*-bis[4-(octyloxy)phenyl]-4-(4,4,5,5-tetramethyl-1,3,2-dioxaborolan-2-yl)aniline similarly as described for compound **3a**. Purple solid, yield 76% (90 mg). ^{1}H NMR (400 MHz, $CDCl_3$, *δ* ppm): 8.55 (d, 1H, *J* = 1.3 Hz), 8.50 (d, 1H, *J* = 1.3 Hz), 8.27 (d, 2H, *J* = 8.5 Hz), 8.12 (d, 2H, *J* = 8.5 Hz), 7.94 (d, 2H, *J* = 8.8 Hz), 7.11 (d, 4H, *J* = 8.8 Hz), 7.00 (d, 2H, *J* = 8.8 Hz), 6.85 (d, 4H, *J* = 8.9 Hz), 3.94 (m, 7H), 1.85-1.70 (m, 4H), 1.40-1.22 (m, 20H), 0.88 (t, 6H, *J* = 5.6 Hz). ^{13}C NMR (100 MHz, $CDCl_3$, *δ* ppm): 167.2, 156.1, 149.4, 144.8, 143.8, 141.3, 140.2, 139.8, 137.9, 135.9, 130.4, 129.2, 128.6, 127.3, 124.3, 119.9, 115.6, 68.5, 52.4, 32.1, 29.6, 29.5, 26.3, 22.9, 14.4. HRMS: m/z calcd for $C_{48}H_{55}N_3O_4S$, 769.3993; found 769.3905.

Synthesis of 4-(7-(4-(trimethylsilyl)phenyl)thieno[3,4-*b*]pyrazin-5-yl)benzaldehyde (5a)

Compound **5a** was synthesized via Suzuki coupling between compound **3a** and 4-trimethylsilylphenylboronic acid similarly as described for compound **3a**. Orange solid, yield 80% (91 mg). ^{1}H NMR (400 MHz, $CDCl_3$, *δ* ppm): 10.04 (s, 1H), 8.60 (d, 2H, *J* = 1.4 Hz), 8.58 (d, 2H, *J* = 1.4 Hz), 8.40 (d, 2H, *J* = 8.4 Hz), 8.11 (d, 2H, *J* = 8.1 Hz), 7.98 (d, 2H, *J* = 8.3 Hz), 7.67 (d, 2H, *J* = 8.2 Hz), 0.32 (s, 9H). ^{13}C NMR (100 MHz, $CDCl_3$, *δ* ppm): 191.8, 145.0, 144.6, 141.7, 141.6, 140.7, 139.1, 135.6, 135.3, 134.3, 132.9, 130.5, 130.2, 128.2, 127.8, 1.0. HRMS: m/z calcd for $C_{22}H_{20}N_2OSSi$, 389.1099; found 389.1135.

Synthesis of methyl 4-(7-(4-(trimethylsilyl)phenyl)thieno[3,4-*b*]pyrazin-5-yl)benzoate (5b)

Compound **5b** was synthesized via Suzuki coupling between compound **3b** and 4-trimethylsilylphenylboronic acid similarly as described for compound **3a**. Orange solid, yield 85% (86 mg). ^{1}H NMR (400 MHz, $CDCl_3$, *δ* ppm): 8.60 (d, 2H, *J* = 3.8 Hz), 8.31 (d, 2H, *J* = 8.4 Hz), 8.17 (d, 2H, *J* = 8.4 Hz), 8.13 (d, 2H, *J* = 7.9 Hz), 7.68 (d, 2H, *J* = 7.8 Hz), 0.34 (s, 9H). ^{13}C NMR (100 MHz, $CDCl_3$, *δ* ppm): 167.0, 144.9, 144.6, 141.5, 140.6, 137.6, 134.2, 133.0, 130.4, 127.8, 52.4, 0.0. HRMS: m/z calcd for $C_{23}H_{22}N_2O_2SSi$, 419.1205; found 419.1249.

Synthesis of 4-(7-(4-iodophenyl)thieno[3,4-*b*]pyrazin-5-yl)benzaldehyde (6a)

Under a nitrogen atmosphere, 1 mol/L ICl in dichloromethane (0.2 mL) was added to 10 mL CH_2Cl_2 solution containing 80 mg compound **5a** (0.22 mmol). After the mixture was stirred at room temperature for 3 h, the solution was washed with dilute sodium hydroxide for three times. The organic solution was washed with brine and dried with anhydrous sodium sulfate. The solvent was removed with a rotary evaporator, and the residue was red solid. ^{1}H NMR (400 MHz, $CDCl_3$, *δ* ppm): 10.04 (s, 1H), 8.59 (d, 1H, *J* = 1.4 Hz), 8.60 (d, 1H, *J* = 1.4 Hz), 8.38 (d, 2H, *J* = 8.3 Hz), 7.98 (d, 2H, *J* = 8.4 Hz). 7.92 (d, 2H, *J* = 8.6 Hz), 7.82 (d, 2H, *J* = 8.6 Hz). ^{13}C NMR (100 MHz, $CDCl_3$, *δ* ppm): 191.8, 145.1, 144.8, 138.8, 138.4, 135.4, 132.2, 130.6, 129.9, 128.3, 123.6, 94.7. HRMS: m/z calcd for $C_{19}H_{12}IN_2OS$, 442.9715; found 442.9703.

Synthesis methyl 4-(7-(4-iodophenyl)thieno[3,4-*b*]pyrazin-5-yl)benzoate (6b)

Compound **6b** was synthesized from compound **5b** similarly as described for compound **5a**. ^{1}H NMR (400 MHz, $CDCl_3$, *δ* ppm): 8.58 (d, 1H, *J* = 1.4 Hz), 8.56 (d, 1H, *J* = 1.4 Hz), 8.25 (d, 2H, *J* = 8.3 Hz), 8.12 (d, 2H, *J* = 8.4 Hz). 7.90 (d, 2H, *J* = 8.7 Hz), 7.81 (d, 2H, *J* = 8.6 Hz), 3.95 (s, 3H). ^{13}C NMR (100 MHz, $CDCl_3$, *δ* ppm): 167.0, 144.9, 144.7, 141.2, 138.3, 137.3, 132.3, 130.4, 129.9, 129.4, 127.8, 94.4, 52.5. HRMS: m/z calcd for $C_{20}H_{14}IN_2O_2S$, 472.9821; found 472.9756.

Synthesis of 4-(7-(4'-(bis(4-(octyloxy)phenyl)amino)-[1,1'-biphenyl]-4-yl)thieno[3,4-*b*]pyrazin-5-yl)benzaldehyde (7a)

Compound **7a** was synthesized via Suzuki coupling between compound **6a** and *N*,*N*-bis[4-(octyloxy)phenyl]-4-(4,4,5,5-tetramethyl-1,3,2-dioxaborolan-2-yl)aniline similarly as described for compound **3a**. Red solid, yield 60% (107 mg). ^{1}H NMR (400 MHz, $CDCl_3$, *δ* ppm): 10.04 (s, 1H), 8.59 (d, 2H, *J* = 2.7 Hz), 8.14 (d, 2H, *J* = 8.3 Hz), 8.20 (d, 2H, *J* = 8.3 Hz), 7.99 (d, 2H, *J* = 8.3 Hz), 7.69 (d, 2H, *J* = 8.3 Hz), 7.47 (d, 2H, *J* = 8.6 Hz), 7.09 (d, 4H, *J* = 8.6 Hz), 7.00 (d, 2H, *J* = 8.2 Hz), 6.94 (d, 4H, *J* = 8.7 Hz), 3.94 (t, 4H, *J* = 6.5 Hz), 1.78 (m, 4H), 1.42-1.24 (m, 20H), 0.88 (t, 6H, *J* = 5.6 Hz). ^{13}C NMR (100 MHz, $CDCl_3$, *δ* ppm):

191.8, 155.9, 148.9, 145.0, 144.4, 141.7, 141.3, 140.7,140.6, 139.2, 135.6, 135.2, 130.8, 130.5, 129.5, 128.8, 128.1, 127.6, 127.0, 120.5, 115.6, 68.5, 32.1, 29.6, 29.5, 26.3, 22.9, 14.3. HRMS: m/z calcd for $C_{53}H_{57}N_3O_3S$, 815.4121; found 815.4129.

Synthesis of methyl 4-(7-(4'-(bis(4-(octyloxy)phenyl)amino)-[1,1'-biphenyl]-4-yl)thieno[3,4-*b*]pyrazin-5-yl)benzoate (7b)

Compound **7b** was synthesized via Suzuki coupling between compound **6b** and *N*,*N*-bis[4-(octyloxy)phenyl]-4-(4,4,5,5-tetramethyl-1,3,2-dioxaborolan-2-yl)aniline similarly as described for compound **3a**. Red solid, yield 62% (90 mg). ^{1}H NMR (400 MHz, $CDCl_3$, δ ppm): 8.55 (s, 1H), 8.52 (d, 1H, *J* = 1.3 Hz), 8.28 (d, 2H, *J* = 7.4 Hz), 8.18 (d, 2H, *J* = 7.7 Hz), 8.13 (d, 2H, *J* = 7.6 Hz), 7.67 (d,2H, *J* = 8.1 Hz), 7.09 (d, 4H, *J* = 8.4 Hz), 7.00 (d, 2H, *J* = 8.2 Hz), 6.85 (d, 4H, *J* = 8.3 Hz), 3.94 (m, 7H), 1.84-1.74 (m, 2H), 1.37-1.25 (m, 10H), 0.90 (t, 6H, *J* = 4.0 Hz). ^{13}C NMR (100 MHz, $CDCl_3$, δ ppm): 167.0, 155.9, 148.8, 144.8, 144.3, 141.1, 140.7, 140.5, 137.6, 131.9, 130.9, 130.4, 129.0, 128.7, 127.7, 127.5, 127.0, 120.5, 115.6, 68.5, 53.4, 32.1, 29.6, 29.5, 16.3, 22.9, 14.3. HRMS: m/z calcd for $C_{54}H_{59}N_3O_4S$, 845.4226; found 845.4239.

Synthesis of sensitizer FNE64

Under a nitrogen atmosphere, a mixture of compound **4a** (100 mg, 0.14 mmol) with cyanoacetic acid (37 mg, 0.42 mmol) in acetonitrile (15 mL) was refluxed in the presence of piperidine (0.3 mL) for 12 h. After cooling, the mixture was diluted with CH_2Cl_2, and washed with water and brine, dried over anhydrous sodium sulfate. The solvent was removed with a rotary evaporator, and the crude product was purified by flash column chromatography (silica gel, DCM/methanol = 10/1, v/v). Dark blue solid was obtained with a yield of 70% (76 mg). ^{1}H NMR (400 MHz, DMSO, δ ppm): 8.64 (s, 1H), 8.58 (s, 1H), 8.32 (d, 2H, *J* = 8.3 Hz), 8.21 (s, 1H), 8.05 (d, 2H, *J* = 8.3 Hz), 7.93 (d, 2H, *J* = 8.3 Hz), 7.03 (d, 4H, *J* = 8.7 Hz), 6.88 (d, 4H, *J* = 8.8 Hz), 6.79 (d, 2H, *J* = 8.6 Hz), 3.90 (t, 4H, *J* = 6.3 Hz), 1.72-1.64 (m, 2H), 1.31-1.27 (m, 10H), 0.84 (t, 6H, *J* = 6.0 Hz). ^{13}C NMR (100 MHz, $CDCl_3$, δ ppm): 156.2, 149.3, 144.5, 143.5, 141.8, 140.0, 139.7, 138.2, 132.0, 130.1, 129.1, 127.4, 124.1, 119.6, 115.6, 68.5, 32.1, 29.7, 29.6, 29.5, 26.3, 22.9, 14.4. HRMS: m/z calcd for $C_{50}H_{54}N_4O_4S$, 806.3866; found 806.3853.

Synthesis of sensitizer FNE65

Under a nitrogen atmosphere, a mixture of compound **4b** (70 mg, 0.12 mmol) and LiOH (10 mg, 0.42 mmol) in a mixed solution of 10 mL THF, 3 mL methanol, and 3 mL water was refluxed in the presence of tetrabutylammonium iodide (20 mg, 0.05 mmol) for 6 h. After cooling to room temperature, the solvent was removed with a rotary evaporator and the residue was dissolved in water. The aqueous portion was acidified to pH = 2 with hydrochloric acid and extracted with CH_2Cl_2. The combined CH_2Cl_2 extracts were dried with anhydrous sodium sulfate. The solvent was removed with a rotary evaporator, and the crude product was purified by flash column chromatography (silica gel, DCM/methanol = 10/1, v/v). A purple solid was obtained with a yield of 66% (60 mg). ^{1}H NMR (400 MHz, DMSO, δ ppm): 8.60 (s, 1H), 8.53 (s, 1H), 8.23 (d, 2H, *J* = 8.4 Hz), 7.98 (d, 2H, *J* = 8.4 Hz), 7.91 (d, 2H, *J* = 8.7 Hz), 6.99 (d, 4H, *J* = 8.7 Hz), 6.84 (d, 4H, *J* = 8.8 Hz), 6.77 (d, 4H, *J* = 8.7 Hz), 3.86 (t, 4H, *J* = 6.3 Hz), 1.58-1.70 (m, 2H), 1.14-1.28 (m, 20H), 0.81 (t, 6H, *J* = 6.0 Hz). ^{13}C NMR (100 MHz, $CDCl_3$, δ ppm): 171.2, 156.2, 149.4, 144.8, 143.8, 141.5, 140.2, 139.8, 138.6, 136.1, 130.9, 129.2, 127.8, 127.4, 119.9, 115.6, 68.5, 32.1, 29.6, 29.5, 26.3, 22.9, 14.4. HRMS: m/z calcd for $C_{47}H_{53}N_3O_4S$, 755.3757; found 755.3725.

Synthesis of sensitizer FNE66

Compound **FNE66** was synthesized from compound **7a** similarly as described for compound **FNE64**. Dark red solid, yield 65% (65 mg). ^{1}H NMR (400 MHz, DMSO, δ ppm): 8.65 (d, 2H, *J* = 5.7 Hz), 8.31 (d, 2H, *J* = 8.2 Hz), 8.17 (d, 2H, *J* = 8.2 Hz), 8.01 (d, 2H, *J* = 8.2 Hz), 7.68 (d, 2H, *J* = 8.4 Hz), 7.51 (d, 2H, *J* = 8.6 Hz), 6.98 (d, 4H, *J* = 8.8 Hz), 6.85 (d, 4H, *J* = 8.7 Hz), 6.81 (d, 2H, *J* = 8.5 Hz), 3.91 (t, 4H, *J* = 6.4 Hz), 1.70-1.62 (m, 4H), 1.16-1.28 (m, 20H), 0.81 (t, 6H, *J* = 6.4 Hz). ^{13}C NMR (100 MHz, $CDCl_3$, δ ppm): 155.6, 152.1, 148.3, 143.0, 140.7, 135.4, 131.8, 129.2, 128.7, 128.4, 128.0, 127.3, 126.8, 126.4, 125.5, 125.0, 124.2, 123.7, 120.6, 116.1, 115.4, 114.3, 114.0, 68.4, 32.1, 29.9, 29.8, 29.7, 26.4, 22.9, 14.9. HRMS: m/z calcd for $C_{56}H_{58}N_4O_4S$, 882.4179; found 882.4123.

Synthesis of compound FNE67

Compound **FNE67** was synthesized from compound **7b** similarly as described for compound **FNE65**. Red solid, yield 60% (55 mg). ^{1}H NMR (400 MHz, DMSO, δ ppm): 8.65 (d, 2H, *J* = 7.7 Hz), 8.28 (d, 2H, *J* = 8.4 Hz), 8.18 (d, 2H, *J* = 8.4 Hz), 8.03 (d, 2H, *J* = 8.5 Hz), 7.68 (d, 2H, *J* = 8.5 Hz), 7.51 (d, 2H, *J* = 8.7 Hz), 6.99 (d, 4H, *J* = 8.8 Hz), 6.86 (d, 4H, *J* = 8.9 Hz), 6.82 (d, 2H, *J* = 8.8 Hz), 3.88 (t, 4H, *J* = 6.4 Hz), 1.72-1.60 (m, 4H), 1.32-1.15 (m, 20H), 0.83 (t, 6H, *J* = 7.0 Hz). ^{13}C NMR (100 MHz, $CDCl_3$, δ ppm): 171.0, 155.8, 148.8, 144.7, 144.2, 141.2, 140.9, 140.7, 140.4, 138.0, 134.6, 128.7, 128.5, 127.5, 127.4, 127.3, 127.0, 126.9, 120.5, 115.5, 68.5, 32.1, 29.7, 29.6, 29.5, 26.4, 22.9, 14.4. HRMS: m/z calcd for $C_{53}H_{57}N_3O_4S$, 831.4070; found 831.4041.

Characterizations

^{1}H NMR (400 MHz) and ^{13}C NMR (100 MHz) spectra were measured on a Varian Mercury Plus-400 spectrometer. The splitting patterns are designated as follows: s (singlet); d (doublet); t (triplet); and m (multiplet). The UV-vis absorption spectra of the sensitizers in dilute toluene solutions and on TiO_2 films were measured with a Shimadzu UV–2550PC UV-vis-NIR spectrophotometer. The film thickness was measured by a surface profiler (Veeco Dektak 150, USA). The cyclic voltammetry (CV) were determined with an CHI660E electrochemical workstation using a typical three-electrode electrochemical cell with dye adsorbed TiO_2 film on conductive glass as the working electrode, a Pt wire as the counter electrode, and an Ag/Ag^+ electrode as the reference electrode, and 0.1 M tetrabutylammonium hexafluorophosphate ($TBAPF_6$) was used as the supporting electrolyte in water-free acetonitrile. The potential of the reference electrode was calibrated by ferrocene, and all potentials mentioned in this work are against normal hydrogen electrode (NHE).

DSSC fabrication and photovoltaic performance measurements

TiO_2 films were fabricated by a screen printing on conducting glass substrate. The films were sintered at 500 °C for 2 h to achieve good necking of neighboring TiO_2 particles. The sintered films were further treated with 0.05 M $TiCl_4$ aqueous solution at 70 °C for 30 min, then washed with water, and annealed at 450 °C for 30 min. When cooled down at around 120 °C, the TiO_2 electrodes were dipped in the solution of dye with 0.3 mM in concentration in toluene/EtOH (v/v, 7/3) for 24 h at room temperature for complete dye adsorption. TiO_2 on conductive glass as the working electrode and Pt-coated conductive glass as the counter electrode were assembled into a sealed sandwich solar cell with a thermoplastic frame (Surlyn, 30 μm thick). A quasi-solid-state gel electrolyte was prepared by mixing 5 wt% poly(vinylidenefluoride-co-hexafluoropropylene) (PVDF-HFP) with a redox solution containing 0.1 M LiI, 0.1 M I_2 , 0/0.1/0.2/0.3/0.4/0.5 M tert-butylpyridine (TBP), and 0.6 M 1,2-dimethyl-3-propylimidazolium iodide (DMPImI) in 3-methoxypropionitrile (MPN) under heating at 100 °C until all solids were dissolved. After introducing the hot gel solution into the internal space of the cell from the two holes predrilled on the back of the counter electrode, a uniform motionless polymer gel layer was formed between the working and the counter electrodes, and then the holes were sealed with a Surlyn film covered with a thin glass slide under heat. The quasi-solid-state DSSCs based on the resulting sensitizers (0.3 mM) with coadsorption of deoxycholic acid were constructed according to our previously reported method.[4c] The active area is 0.25 cm^2. The current density–voltage (*J–V*) characteristics of the DSSCs were measured by recording *J–V* curves using a Keithley 2420 source meter under the illumination of AM1.5G simulated solar light coming from a solar simulator (Sol3A equipped with a 450 W Xe lamp and an AM1.5G filter, Newport). The light intensity was calibrated with a standard silicon solar cell (Newport 91150). The electron lifetimes were measured with intensity modulated photovoltage spectroscopy (IMVS), whereas charge densities at open-circuit were measured using the charge extraction technique. IMVS analysis and charge extraction were carried out on an electrochemical workstation (Zahner XPOT, Germany), which includes a white light emitting diode and corresponding control system. The intensity modulated spectra were measured at room temperature with light intensity ranging from 20 to 120 W m^{-2}, in modulation frequency ranging from 0.1 Hz to 10 kHz, and with modulation amplitude less than 5% of the light intensity. Action spectra of the incident monochromatic photon-to-electron conversion efficiency (IPCE) for the solar cells were recorded using an SM-250 system (Bunkoh-Keiki, Japan). The intensity of monochromatic light was measured with a Si detector (S1337-1010BQ).

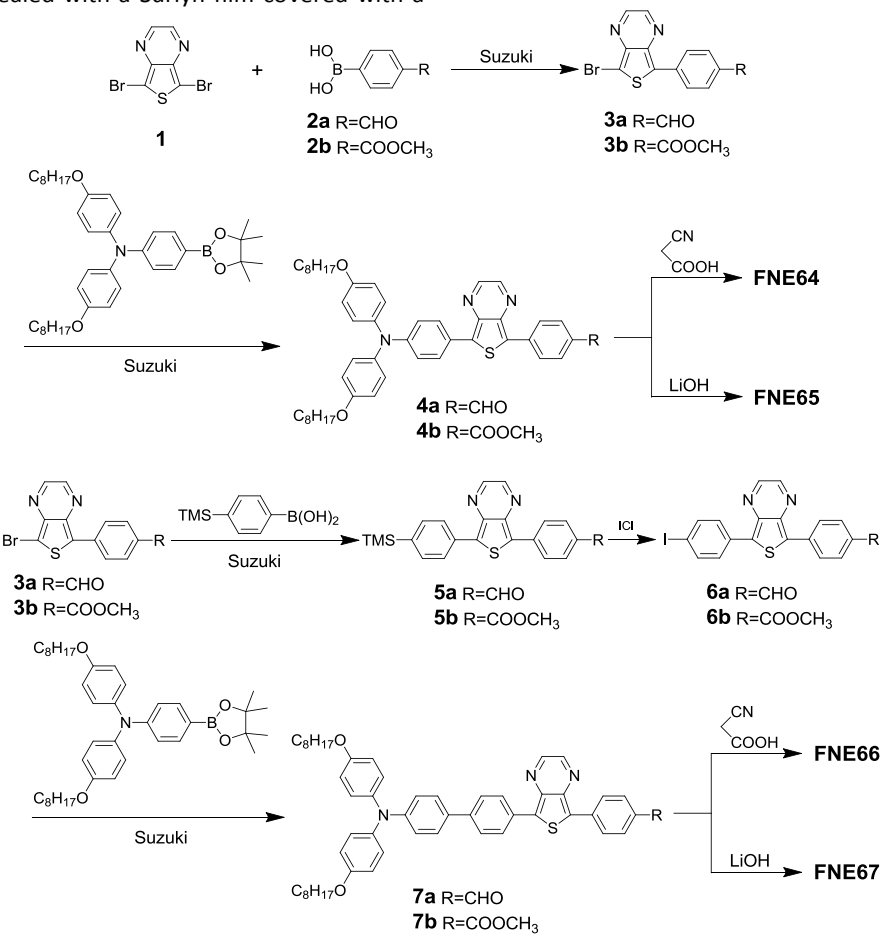

Scheme 1. Synthetic route for sensitizer **FNE64**, **FNE65**, **FNE66**, and **FNE67**.

Results and Discussion

Synthesis of Sensitizers.

The approach towards sensitizers **FNE64**-**FNE67** is depicted in Scheme 1. The synthesis of the four target sensitizers started from 2,5-dibromothieno[3,4-*b*]pyrazine (**1**)[14] which was firstly converted to compound **3a** and **3b** by an asymmetrical Suzuki coupling[15] with 4-formylbenzeneboronic acid (**2a**) and 4-methoxycarbonylbenzeneboronic acid (**2b**), respectively. Via a further Suzuki coupling with *N*,*N*-bis[4-(octyloxy)phenyl]-4-(4,4,5,5-tetramethyl-1,3,2-dioxaborolan-2-yl)aniline, electron donating group was introduced and precursors **4a** and **4b** were provided. Compared with reference **FNE32**, octyloxy substituted triarylamine was incorporated as electron donor instead of triphenylamine due to its unique merits, such as stronger electron donating capability, endowing sensitizers sufficient solubility, and suppressing intermolecular aggregation on TiO_2 film and thus retarding charge recombination in DSSCs. On the other hand, a Suzuki coupling between intermediate compound **3a**/**3b** and 4-trimethylsilylphenylboronic acid produced TMS-protected compounds **5a** and **5b**, respectively, which were further transferred to iodides **6a** and **6b** by reaction with ICl.[16] Similarly, electron donating group was incorporated via a Suzuki coupling, which provides precursors **7a** and **7b**. Afterwards, precursors **4a** and **7a** were converted to sensitizers **FNE64** and **FNE66** by Knoevenagel condensation[17] with cyanoacetic acid through refluxing acetonitrile in the presence of piperidine, while sensitizers **FNE65** and **FNE67** were obtained by de-esterification from precursors **4b** and **7b** through refluxing with LiOH.[18] All the target dye sensitizers were characterized by ^{1}H NMR, ^{13}C NMR, and HRMS spectroscopies, and were found to be consistent with the proposed structures.

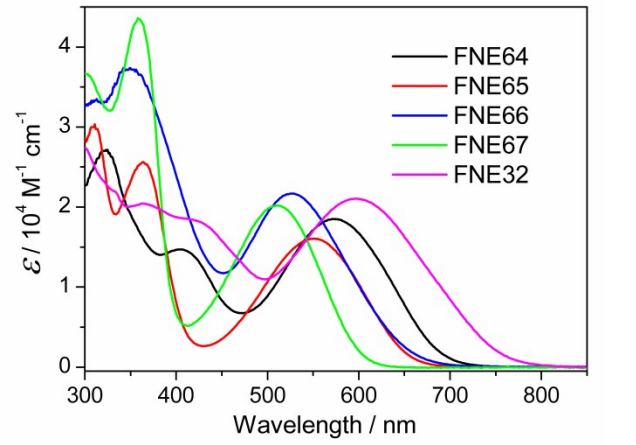

Fig. 2 UV-vis absorption spectra of sensitizers **FNE32**, **FNE64**, **FNE65**, **FNE66**, and **FNE67** in dilute toluene solutions.

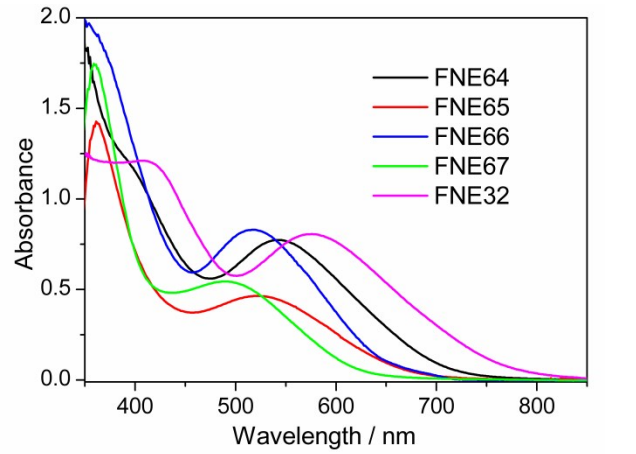

Fig. 3 UV-vis absorption spectra of sensitizers **FNE32**, **FNE64**, **FNE65**, **FNE66**, and **FNE67** on 1.5 μm TiO_2 films.

Table 1. UV-vis absorption and electrochemical properties of sensitizers **FNE32**, **FNE60**, **FNE61**, **FNE62**, and **FNE63**.

Dye	Absorption			Exp/Cal HOMO[b]	E_g	Exp/Cal LUMO[b]
	λ_{max}[a]	ε[a]	λ_{max} on TiO_2			
	nm	M^{-1} cm^{-1}	nm	V *vs.* NHE	eV	V *vs.* NHE
FNE64	572	1.9×10^4	543	1.00/1.79	1.75	-0.75/-1.25
FNE65	549	1.6×10^4	524	0.97/1.72	1.83	-0.86/-1.39
FNE66	525	2.2×10^4	518	0.97/1.66	1.88	-0.91/-1.50
FNE67	511	2.0×10^4	492	1.03/1.73	1.99	-0.96/-1.56
FNE32	596	2.2×10^4	576	0.97/1.71	1.61	-0.64/-1.17

[a] Absorption peaks (λ_{max}) and molar extinction coefficients (ε) were measured in toluene solutions (~10^{-5} M). [b] The potentials (*vs.* NHE) were calibrated with ferrocene.

Photophysical Properties

The UV-Vis absorption spectra of the four sensitizers in dilute toluene solutions (*ca.* 10^{-5} M) are depicted in **Fig. 2** and the corresponding photophysical data are summarized in **Table 1**. Similar to reference **FNE32**, all the thieno[3,4-*b*]pyrazine based sensitizers exhibit their major electronic absorption bands in the visible region due to the intramolecular charge transfer (ICT) from the electron donating moiety to the electron accepting moiety.[19] Additionally, another absorption band can be observed for all dyes in the ultraviolet region, which is assigned to the π–π* electron transition of the conjugated backbone. Compared with the maximum absorption band of **FNE32**,[10] the absorption spectra of

sensitizer **FNE64** displays the maximum absorption wavelength at 572 nm with a hypsochromic shift of 24 nm, which is obviously owing to the shortened effective conjugation length. When the cyanoacetic acid in **FNE64** is replaced by carboxylic acid group, a much weaker electron acceptor, **FNE65** demonstrates the maximum absorption wavelength at 549 nm with a hypsochromic shift of 23 nm as compared with **FNE64**, due to the much weaker electron-withdrawing property of carboxylic acid in comparison to cyanoacrylic acid which results in the weakened ICT interactions and higher energy absorption. Moreover, when an auxiliary benzene ring is inserted between the triarylamine and thieno[3,4-*b*]pyrazine unit in **FNE64**, sensitizer **FNE66** displays the absorption maximum wavelength at 525 nm with a more significant hypsochromic shift of 47 nm and increased molar extinction coefficient in comparison to that for sensitizer **FNE64**. In general, extending the conjugation by inserting a benzene ring can bathochromically shift the maximum absorption wavelength. However, in comparison to sensitizer **FNE64**, a significant hypsochromic shift of 47 nm is observed for the absorption maximum of sensitizer **FNE66**. Similar phenomena[13] have been previously reported and can be explained by the following two factors. The first is the steric hindrance between benzene ring and neighbored functional groups, which induces a more twisted molecular skeleton in sensitizer **FNE66** as compared with **FNE64**. Another reason is the enhanced distance between the electron donor and acceptor, which probably weakens the ICT interactions and results in the hypsochromically shifted absorption maximum. It should be noted that a hypsochromic shift of 71 nm can be observed for the absorption maximum of sensitizer **FNE66** as compared with reference sensitizer **FNE32**. This is obviously due to the much less electron donating capability of benzene ring as compared with thiophene ring. Furthermore, when the cyanoacrylic acid unit in sensitizer **FNE66** is replaced by carboxylic acid, sensitizer **FNE67** exhibits the maximum absorption wavelength at 511 nm with a hypsochromic shift of 14 nm in comparison to that for sensitizer **FNE66**, which is similar to those for sensitizers **FNE64** and **FNE65**. Moreover, in comparison to sensitizers **FNE64** and **FNE65** with D-A-π-A configuration, sensitizers **FNE66** and **FNE67** with D-π-A-π-A configuration exhibit hypsochromically shifted absorption maxima by 47 and 38 nm, respectively, which indicates that D-A-π-A framework is superior to D-π-A-π-A configuration in expanding the absorption spectrum and enhancing the light-harvesting capability. This is inconsistent with our previously reported result[12c] and because of their different π spacers in two cases.

The UV-vis absorption spectra of the target sensitizers on TiO_2 films are recorded and shown in **Fig. 3**. Sensitizers **FNE64**, **FNE65**, **FNE66**, and **FNE67** demonstrate the maximum absorption wavelength at 543, 524, 518, and 492 nm, respectively, which displays the same trend as those in toluene solutions. A slight hypsochromic shift of 29, 25, 7, and 19 nm, respectively, can be found for the absorption maxima of dye-loaded TiO_2 films with respect to those in toluene solutions. Such hypsochromic shifts of the absorption spectra for organic dyes absorbed on the TiO_2 films have also been observed in other D-(π)-A-π-A featured organic dyes and can be owing to the deprotonation of the carboxylic acid.[11] To further investigate the influence of the anchoring group on the dye-loading amount, the adsorption amounts of sensitizers **FNE64**, **FNE65**, **FNE66**, and **FNE67** are measured to be 1.80×10^{-8}, 1.27×10^{-8}, 1.65×10^{-8}, and 1.18×10^{-8} mol cm^{-2} μm^{-1}, respectively. It can be found that the surface concentration of cyanoacrylic acid based sensitizer is slightly higher than that for carboxylic acid based sensitizer, which can probably owing to the relatively stronger binding effect of cyanoacrylic acid on TiO_2 semiconductor.

Electrochemical Properties.

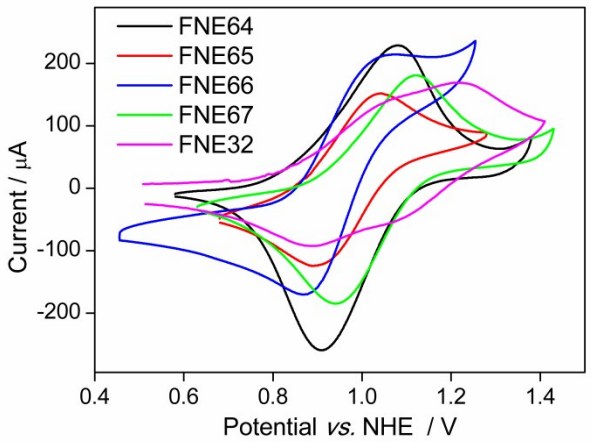

Fig. 4 Cyclic voltammograms of the dye-loaded TiO_2 films (0.25 cm^2).

To further investigate the energy levels of the target sensitizers and evaluate the possibility of the dye regeneration and the photo-generated electron injection, cyclic voltammetry (CV) was carried out in a typical three-electrode electrochemical cell with TiO_2 films stained with the organic sensitizer as the working electrode in a solution of tetrabutylammonium hexafluorophosphate (0.1 M) in water-free acetonitrile with a scan rate of 50 mV s^{-1} (**Fig. 4**). The data are presented in **Table 1**. The observed oxidation potentials, corresponding to the HOMO energy levels of sensitizers **FNE32**, **FNE64**, **FNE65**, **FNE66** and **FNE67**, are determined to be 1.00, 0.97, 0.97 and 1.03 V (*vs.* NHE, same below), respectively, which are more positive than the redox potential of the I^-/I_3^- redox couples (~0.4 V),[20] indicating that the reduction of oxidized dyes with I^- ions is thermodynamically feasible. The close HOMO values for these organic sensitizers root in the oxidation of the same triarylamine moiety. It should be noted that electrochemistry measures the ionization potential and electron affinity. The HOMO and LUMO are just theoretical constructs but still valid to estimate the energy gap.[21] Correspondingly, the LUMO energy level was calculated from equation (1),

$$\text{LUMO} = \text{HOMO} - \Delta E \qquad (1)$$

where ΔE is the energy gap between the HOMO and LUMO levels and derived from the wavelength at 10% maximum absorption intensity for the dye-loaded TiO_2 film.[22] The LUMO

energy levels of dyes **FNE32**, **FNE64**, **FNE65**, **FNE66** and **FNE67**, are calculated to be -0.64, -0.75, -0.86, -0.91 and -0.96 V, respectively. Generally, it is considered that a minimum offset of around 0.3 eV between the LUMO of the organic sensitizer and the CB edge of TiO_2 electrode (-0.5 V), [20] which determines the driving force for the excited electron injection, is needed to ensure fast and efficient electron injection. As compared with **FNE32** with LUMO level of -0.64 V where the driving force for electron injection from the oxidized dye molecules into the TiO_2 is insufficient, the target thieno[3,4-*b*]pyrazine based sensitizers have gradually upward shifted the LUMO levels, which results in an increased capability of photo-generated electron injection from the excited organic dye to the TiO_2 semiconductor. Moreover, in comparison sensitizers **FNE64** and **FNE65** with single phenylene unit, sensitizers **FNE66** and **FNE67** with double phenylene units have successfully lifted up the LUMO levels. This is due to the fact that the HOMO partially delocalizes on the phenylene units, which therefore weakens the electron-withdrawing property of thieno[3,4-*b*]pyrazine group and therefore lifts up the LUMO levels. Therefore, it can be concluded that the LUMO energy levels of D-(π)-A-π-A featured organic sensitizers can be precisely tuned upon the optimization of either the π-conjugation spacer or the anchoring group.

Theoretical Approach

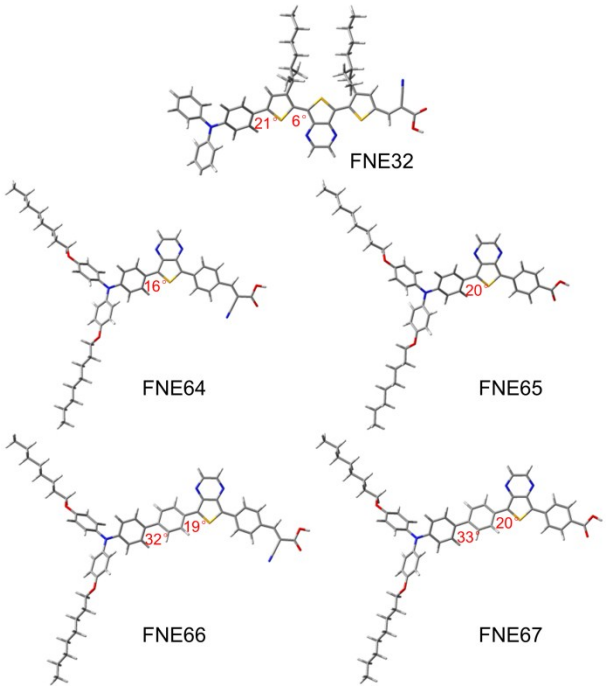

Fig. 5 Optimized ground state geometry and related dihedral angels for sensitizers **FNE32**, **FNE64**, **FNE65**, **FNE66**, and **FNE67**.

Density functional theory (DFT) calculations of the target sensitizers are performed at the B3LYP/6-31G(d) level of theory[23] to gain insight into the geometrical structures and the frontier orbitals. As shown in the optimized conformation (**Fig. 5**), the dihedral angles between thieno[3,4-*b*]pyrazine unit and the neighboured thiephene ring in sensitizers **FNE32** is calculated to be 6°, which are generalized observation for dihedral angles between two thiophene rings. When the bridged thiephene rings are replaced by benzene rings, the dihedral angles between the thieno[3,4-*b*]pyrazine unit and the neighboured benzene ring are calculated to be 16° and 20°, respectively, for sensitizers **FNE64** and **FNE65**. Moreover, when an auxilary benzene ring is incorporated between the triarylamine and thieno[3,4-*b*]pyrazine unit, the dihedral angles between the benzene ring in the triarylamine moiety and the inserted phenylene unit in sensitizers **FNE66** and **FNE67** increases to 32° and 33°, respectively, which are general dihedral angles between two benzene rings. While the dihedral angles between the thieno[3,4-*b*]pyrazine unit and the neighboured thiophene ring is calculated to be 19° and 20°, respectively, for sensitizers **FNE66** and **FNE67**. It should be noted that when an auxaliary benzene ring is inserted between the triarylamine and thieno[3,4-*b*]pyrazine in sensitizers **FNE64** and **FNE65** with D-A-π-A configuration, a more twisted molecular structure can be observed for both sensitizers **FNE66** and **FNE67** with D-π-A-π-A configuration. Therefore, although the π-conjugation is geometrically extended through the incorporated phenylene unit, a worse

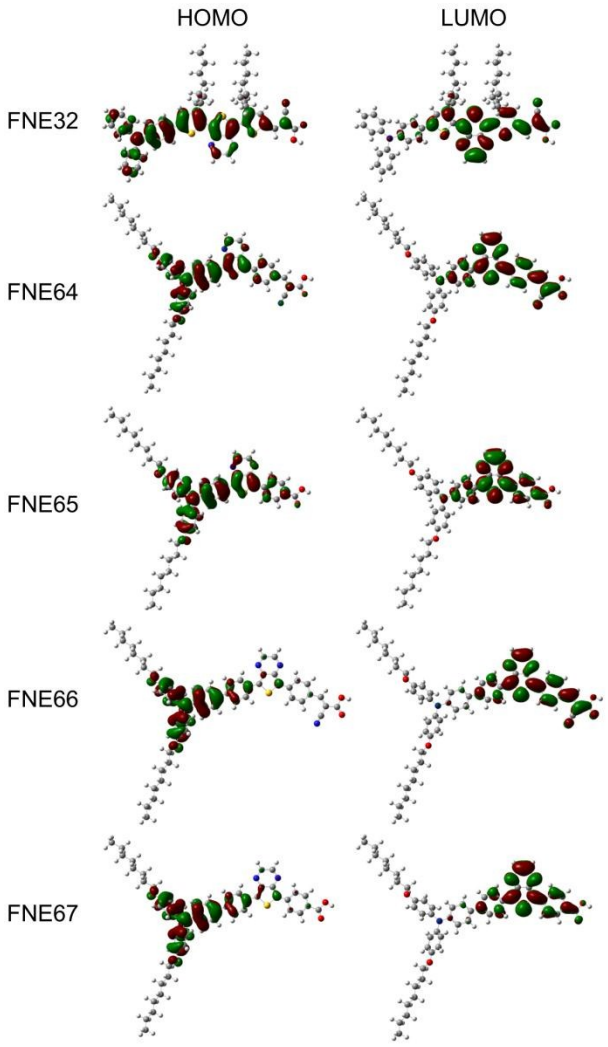

Fig. 6 Calculated frontier molecular orbitals of sensitizers **FNE32**, **FNE64**, **FNE65**, **FNE66**, and **FNE67**.

charge delocalization is found in the D-π-A-π-A featured organic sensitizers with phenylene bridges, which results in the weakend ICT interactions and is consistent with their absorption maxima (**Fig. 2**).

The energy levels and the frontier molecular orbitals of the target sensitizers were also calculated. As listed in Table 1, although the calculated LUMO levels are differed from the experimental ones, the qualitative trends of the theoretical LUMO levels are mostly similar to those experimentally determined ones. **Fig. 6** displays the calculated frontier molecular orbitals of the organic sensitizers. It can be clearly found that for sensitizers **FNE32**, **FNE64**, and **FNE65**, the HOMOs delocalize on the triarylamine moiety with extension to the whole molecular skeleton, while the LUMOs delocalize on the two acceptors and extend to the nitrogen in the triarylamine. The overlap of the HOMOs and LUMOs facilitates the charge transfer from the electron-donating center to the electron-withdrawing center.[24] On the contrary, for sensitizers **FNE66** and **FNE67**, the HOMOs mainly delocalize on the triarylamine moiety and the neighbored phenylene bridge, while the LUMOs mainly delocalize on the two acceptors and two bridged benzene rings. As compared with sensitizers **FNE64** and **FNE65** with D-A-π-A configuration, the different frontier molecular orbital delocalizations on D-π-A-π-A featured sensitizers **FNE66** and **FNE67** indicate differed ICT interactions in these organic sensitizers with similar donors and acceptors. Moreover, for all the sensitizers with either cyanoacrylic acid or carboxylic acid as anchoring group, the LUMOs delocalize over the anchoring acid groups. Thus, upon excitation by the sunlight, the excited electrons may transfer from the triarylamine center to the anchoring group and further possibly into TiO_2 under the condition of sufficient electron injection driving force.

Table 2 Photovoltaic performance for **FNE66** based quasi-solid-state DSSC with different concentrations of TBP in the electrolyte and DCA in the dye bath.

C_{DCA} mM	C_{TBP} M	V_{oc} mV	J_{sc} mA cm^{-2}	*FF* %	η %
0	0.1	576	13.18	63	4.8
5		595	15.18	68	6.1
10		611	17.25	68	7.2
20		608	14.47	64	5.6
10	0	566	13.63	67	5.2
	0.1	611	17.25	68	7.2
	0.2	629	15.60	70	6.9
	0.3	649	15.53	67	6.8
	0.4	652	14.09	70	6.4
	0.5	656	13.71	69	6.2

Solar Cell Performance

The quasi-solid-state DSSCs based on the prepared sensitizers (0.3 mM) were fabricated with a polymer gel electrolyte containing 5% PVDF-HFP (w/w) in MPN. To achieve the best DSSC performance, the content of deoxycholic acid (DCA) in the dye bath and tert-butylpyridine (TBP) in the electrolyte were optimized firstly optimized for **FNE66** based quasi-solid-state DSSC since it provided the best performance in our initial measurement. In general, the utilization of DCA as a coadsorbate,[25] which is simultaneously adsorbed on the TiO_2 electrode during the dye adsorption process, has been proved to be an efficient method to improve the DSSC performance due to the suppression of dye aggregation and prevention of the backward electron transfer. Therefore, the effect of DCA was firstly investigated by mixing various concentrations of DCA with **FNE66** in the dye bath for fabricating sensitized TiO_2 films. The performance data are summarized in **Table 2**. When the concentration of DCA increases from 0 to 10 mM, both open-circuit voltage (V_{oc}) and short-circuit current (J_{sc}) increase upon the addition of DCA in the dye bath. This is obviously stemmed from the coadsorption of the additive DCA, which weakens the intermolecular interactions and thus reduces the charge recombination rate in the quasi-solid-state DSSCs. However, when the DCA concentration increases to 20 mM, both the V_{oc} and J_{sc} values decrease in some extent since the coadsorbed DCA molecules occupy the binding sites on TiO_2 film, inducing in a decrease in the amount of organic dyes loaded on the TiO_2 film.

It is well known that TBP is a commonly used species in the electrolyte to improve the DSSC performance[26] since the coordination between electronegative pyridine and TiO_2 negatively shifts the TiO_2 conduction band edge. Therefore, the content of TBP in the electrolyte was also optimized and it is found to greatly affect the DSSC performance (**Table 3**). When the content of TBP increases from 0 to 0.1 M and further to 0.5 M, the V_{oc} value gradually increases along with the TBP concentration but J_{sc} values achieve the highest at 0.1 M TBP. The increased V_{oc} value is mainly attributed to the negative shift of the conduction band of TiO_2 caused by the adsorption of TBP on the TiO_2 surface. On the other hand, J_{sc} value increases from 13.63 to 17.25 mA cm^{-2} upon addition of 0.1 M TBP, probably owing to the reduced charge recombination rate, and then decreases to 13.71 mA cm^{-2} at 0.5 M TBP due to the reduction of the driving force for the electron injection from the excited dye molecule to the conduction band of titania semiconductor. Therefore, the quasi-solid-state DSSCs based on the target sensitizers with DCA (10 mM) were fabricated using a quasi-solid-state electrolyte containing 0.1 M TBP.

Action spectra of the incident photon-to-current conversion efficiencies (IPCE) as a function of incident wavelength for the quasi-solid-state DSSCs were recorded and shown in **Fig. 7**. The maximum IPCE values for the quasi-solid-state DSSCs increase following the order **FNE32** < **FNE64** < **FNE65** < **FNE66** < **FNE67**. According to the formula (2): [27]

$$\mathrm{IPCE}(\lambda) = \mathrm{LHE}(\lambda) \times \Phi_{inj} \times \Phi_{c} \qquad (2)$$

where $\mathrm{LHE}(\lambda)$ is the light-harvesting efficiency, Φ_{inj} is the electron injection efficiency, and Φ_c is the charge collection efficiency, since the LHE for the dye-loaded 15 μm thick TiO_2 film is close to unity for all the three devices, the much lower

IPCE values for the DSSCs based on **FNE32**, **FNE64**, and **FNE65** are stemmed from their insufficient driving force for electron injection from the excited **FNE32**, **FNE64** or **FNE65** molecules to the TiO_2 conduction band, as revealed by the electrochemcial study. Moreover, compared with the IPCE spectra of the quasi-solid-state DSSCs based on **FNE65** and **FNE67** with carboxylic acid as anchoring group, the quasi-solid-state DSSCs based on **FNE64** and **FNE66** with cyanoacrylic acid as anchoring group display much broader IPCE spectra obviously due to their wider photo-response range, which is consistent with the absorption spectra of the dye loaded TiO_2 films. These results indicate that not only broad absorption spectrum but also suitable energy levels are required for ideal photon-to-current conversion in the DSSCs.

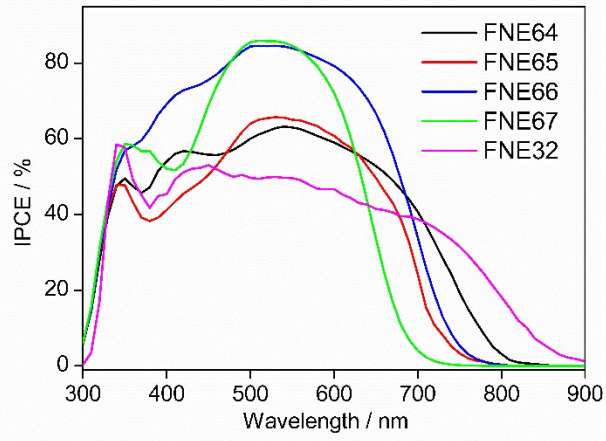

Fig. 7 IPCE spectra for the quasi-solid-state DSSCs based on sensitizers **FNE32**, **FNE64**, **FNE65**, **FNE66**, and **FNE67**.

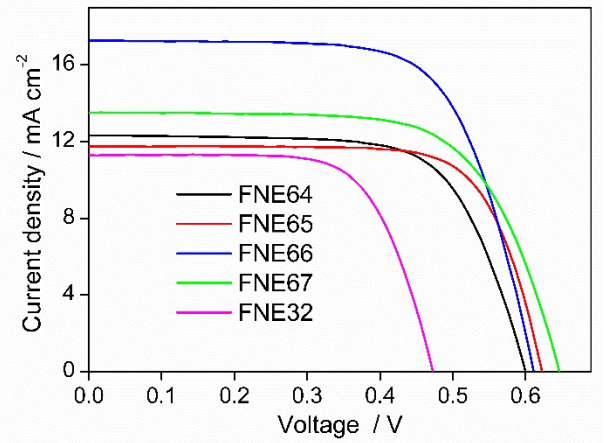

Fig. 8 *J* – *V* curves for the quasi-solid-state DSSCs based on sensitizers **FNE32**, **FNE64**, **FNE65**, **FNE66**, and **FNE67**.

Table 3 Photovoltaic performance of the quasi-solid-state DSSCs based on sensitizers **FNE32**, **FNE64**, **FNE65**, **FNE66**, and **FNE67**.

Sensitizer	V_{oc} mV	J_{sc} mA cm^{-2}	*FF* %	η %
FNE64	599	13.38	69	5.5
FNE65	622	12.55	73	5.7
FNE66	611	17.25	68	7.2
FNE67	646	14.44	67	6.2
FNE32	470	11.29	69	3.7

The current-voltage (*J-V*) characteristics of the quasi-solid-state DSSCs were measured under standard AM1.5G solar light (100 mW cm^{-2}) and displayed in **Fig. 8**. The detailed photovoltaic parameters in terms of J_{sc}, V_{oc}, fill factor (*FF*), and η of each DSSC are listed in **Table 3**. The quasi-solid-state DSSCs based on **FNE64** and **FNE65** produces a J_{sc} of 13.38 and 12.55 mA cm^{-2}, respectively. Upon the incorporation of an additional benzene ring as spacer, sensitizer **FNE66** and **FNE67** based DSSCs provides an improved J_{sc} of 17.25 and 14.44 mA cm^{-2}, respectively. In general, the J_{sc} can be expressed by equation (3):[28]

$$J_{sc} = \frac{hc}{q}\int_{\lambda_1}^{\lambda_2}\frac{P_{AM1.5G}(\lambda)\bullet IPCE(\lambda)\bullet d\lambda}{\lambda} \qquad (3)$$

where *h* is Plank's constant, *c* is the speed of light in vacuum, and λ_1 and λ_2 are the limits of the active spectrum of the DSSC. Therefore, although the absorption spectra of sensitizers **FNE64** and **FNE65** are broadened in comparison to those for sensitizers **FNE66** and **FNE67**, respectively, the latter sensitizer based quasi-solid-state DSSCs produce higher J_{sc} values, which is consistent with the trend of the photo-generated current integrated from the IPCE spectra. It should be noted that all the J_{sc} values of the quasi-solid-state DSSCs based on the four target sensitizers are higher than that for **FNE32** based quasi-solid-state DSSC (11.29 mA cm^{-2}) under its best condition, which is attributed to the improved driving force for electron injection from the excited dye molecules to the TiO_2 semiconductor. Correspondingly, the quasi-solid-state DSSCs based on sensitizers **FNE64**, **FNE65**, **FNE66**, and **FNE67** produced a V_{oc} of 599, 622, 611, and 646 mV, respectively, and a *FF* of 69%, 73%, 68%, and 67%, respectively, corresponding to a η of 5.5%, 5.7%, 7.2%, and 6.2%, respectively.

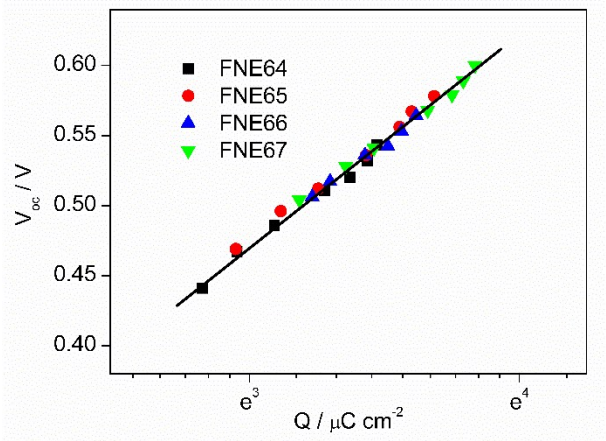

Fig. 9 Charge density at open circuit as a function of V_{oc} for the quasi-solid-state DSSCs based on sensitizers **FNE64**, **FNE65**, **FNE66**, and **FNE67**.

Generally, V_{oc} is defined as the potential difference between the quasi-Fermi potential of electrons (E_{Fermi}) in the titania semiconductor and the redox potential (E_{redox}) of the electrolytes, which could be described by equation (4):[29]

$$V_{oc} = \frac{E_{cb}-E_{redox}}{q} + \beta\frac{kT}{q}\ln\frac{n}{N_{cb}} \qquad (4)$$

where β is a characteristic constant of the TiO_2 tailing states, k is the Boltzmann constant, T is the temperature, q is the elementary charge, and N_{cb} is the total number of conduction band states in the semiconductor, n is the number of electrons in titania semiconductor. Therefore, V_{oc} is judged by the conduction band position of titania semiconductor and the charge recombination rate in the DSSCs. To further explain the V_{oc} difference among the fabricated quasi-solid-state DSSCs, the conduction band edge position of the dye loaded titania films were firstly studied by charge extraction[29] and intensity modulated photovoltage spectroscopy (IMVS) measurements.[31] At constant photo-induced charge density (Q), a higher V_{oc} indicates an upward shift of the conduction band edge, and vice versa. As shown in **Fig. 9** which illustrates the relation between V_{oc} and Q at open circuit for the fabricated quasi-solid-state DSSCs, the V_{oc} values increase linearly with the logarithm of Q for all DSSCs. All the curves for the corresponding devices have almost the same slope (143 mV) and coincide with each other. At a fixed Q, the almost same V_{oc} values for all DSSCs indicate the identical conduction band edge positions. Therefore, it can be concluded that modification of the LUMO levels has no obvious influence on the conduction band edge of titania semiconductors.

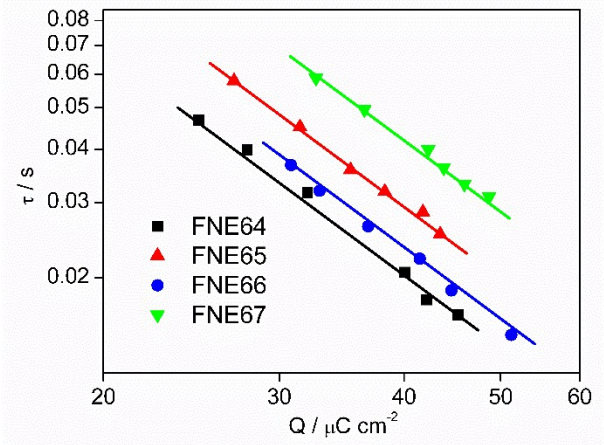

Fig. 10 Electron lifetime as a function of electron density at open circuit for the quasi-solid-state DSSCs based on sensitizers **FNE64**, **FNE65**, **FNE66**, and **FNE67**.

Therefore, the V_{oc} difference can be ascribed to the various charge recombination rates which are related to electron lifetime (τ) in the DSSCs.[32] The electron lifetime was measured by IMVS and obtained from the frequency at the top of the semicircle (f_{min}) according to equation (5): [33]

$$\tau = \frac{1}{2\pi f_{min}} \qquad (5)$$

Fig. 10 shows the electron lifetime as a function of charge density at open circuit. The electron lifetime for a certain DSSCs decreases with charge density following a power law relation with the same slope, suggesting the same charge recombination mechanism in the four quasi-solid-state DSSCs. Moreover, the electron lifetime in the quasi-solid-state DSSCs based on **FNE66** and **FNE67** with D-π-A-π-A structure is much longer at a certain charge density in comparison to that for the DSSC based on D-A-π-A featured **FNE64** and **FNE65**, respectively. This originates from the fact that **FNE66** and **FNE67** with D-π-A-π-A structure with more twisted structures can weaken the intermolecular interactions and thus reduce the charge recombination between electrons in TiO_2 film and electron acceptors in the electrolyte more efficiently than **FNE64** and **FNE65** with D-A-π-A structure. Consequently, when more charge is accumulated in TiO_2, the Fermi level moves upward, resulting in a V_{oc} enhancement (ΔV_{oc}) which is related to the electron density (n) or charge density (Q) changes and follows equation (6): [34]

$$\Delta V_{oc} = m_c \ln\frac{n_2}{n_1} = m_c \ln\frac{Q_2}{Q_1} \qquad (6)$$

At 100 W m^{-2} white LED light, the extracted charge densities are 31, 37, 35, and 44 μC cm^{-2} for the quasi-solid-state DSSCs based on **FNE64**, **FNE65**, **FNE66**, and **FNE67**, respectively. According to equation (6), the V_{oc} gain from **FNE64** sensitized quasi-solid-state DSSC to **FNE65**, **FNE66**, and **FNE67** based DSSCs arising solely from the reduced charge recombination rate and increased charge density is calculated to be 25, 17, and 50 mV, respectively. This is in good agreement with the experimentally observed V_{oc} difference between **FNE64** sensitized quasi-solid-state DSSS and those based on **FNE65** (23 mV), **FNE66** (12 mV), and **FNE67** (47 mV), respectively (**Table 3**).

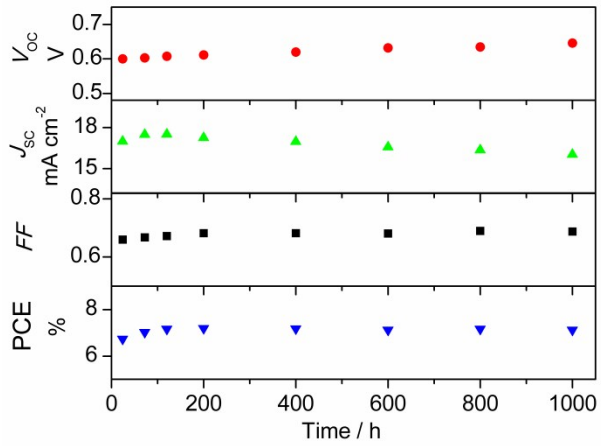

Fig. 11 Evolutions of photovoltaic performance parameters for the quasi-solid-state DSSC based on sensitizer **FNE66** during one sun soaking.

The most advantage of quasi-solid-state DSSC is their stability during long-time operation which is considered as an important requirement for further practical applications.[35] Therefore, the stability of the quasi-solid-state DSSCs based on the resulting sensitizers was recorded over a period of 1000 h under one sun soaking. **Fig. 11** displays the photovoltaic performance parameters of **FNE66** based quasi-solid-state DSSC. It can be found that J_{sc}, V_{oc} and η values slightly improve initially. Flowing, the J_{sc} droped but V_{oc} increased within 5% with sunlight soaking time, while FF and η parameters remained almost constant after 1000 h of one sun soaking, which indicates that sensitizer **FNE66** is sufficiently stable for DSSC applications.

Conclusions

In summary, four organic sensitizers based on thieno[3,4-*b*]pyrazine with different numbers of phenylene bridges and different anchoring groups have been designed and synthesized. Compared with reference **FNE32** whose photo-response range is over 900 nm, either the replacement of thiophene by benzene spacer or the incorporation of carboxylic acid instead of cyanoacrylic acid can lift up the LUMO levels of the organic sensitizers and ensure more efficient electron injection. Although hypsochromically shifted absorption maxima are achieved for the target sensitizers upon energy level optimization, the η value of the quasi-solid-state DSSC based on sensitizer **FNE66** increases by 95% as compared with that for the quasi-solid-state DSSC based on sensitizer **FNE32** with panchromatic absorption. Therefore, at a fixed A', other building blocks in D-(π)-A-π-A featured organic sensitizers can be tuned to optimize the energy levels to ensure sufficient driving force for charge injection and dye regeneration. These results will help us to understand the critical importance of energy level engineering and provide a path for designing organic sensitizers with D-(π)-A-π-A configuration.

Acknowledgements

This work was financially supported by the National Basic Research Program of China (2011CB933302), the National Natural Science Foundation of China (51273045), NCET-12-0122, STCSM (12JC1401500), and Shanghai Leading Academic Discipline Project (B108).

References

1. B. O'Regan and M. Grätzel, *Nature*, 1991, **353**, 737-740.
2. (a) M. K. Nazeeruddin, P. Péchy, T. Renouard, S. M. Zakeeruddin, R. Humphry-Baker, P. Comte, P. Liska, L. Cevey, E. Costa, V. Shklover, L. Spiccia, G. B. Deacon, C. A. Bignozzi and M. Grätzel, *J. Am. Chem. Soc.,* 2001, **123**, 1613-1624; (b) M. K. Nazeeruddin, F. De Angelis, S. Fantacci, A. Selloni, G. Viscardi, P. Liska, S. Ito, B. Takeru and M. Grätzel, *J. Am. Chem. Soc.,* 2005, **127**, 16835-16847; (c) A. Yella, H.-W. Lee, H. N. Tsao, C. Yi, A. K. Chandiran, M. K. Nazeeruddin, E. W.-G. Diau, C.-Y. Yeh, S. M. Zakeeruddin and M. Grätzel, *Science*, 2011, **334**, 629-634; (d) T. Funaki, H. Funakoshi, O. Kitao, N. Onozawa-Komatsuzaki, K. Kasuga, K. Sayama and H. Sugihara, *Angew. Chem. Int. Ed.*, 2012, **51**, 7528-7531; (e) K.-L. Wu, C.-H. Li, Y. Chi, J. N. Clifford, L. Cabau, E. Palomares, Y.-M. Cheng, H.-A. Pan and P.-T. Chou, *J. Am. Chem. Soc.,* 2012, **134**, 7488-7496; (f) L. E. Polander, A. Yella, B. F. E. Curchod, N. Ashari Astani, J. Teuscher, R. Scopelliti, P. Gao, S. Mathew, J.-E. Moser, I. Tavernelli, U. Rothlisberger, M. Grätzel, M. K. Nazeeruddin and J. Frey, *Angew. Chem. Int. Ed.*, 2013, **52**, 8731-8735; (g) J. Luo, M. Xu, R. Li, K.-W. Huang, C. Jiang, Q. Qi, W. Zeng, J. Zhang, C. Chi, P. Wang and J. Wu, *J. Am. Chem. Soc.,* 2014, **136**, 265-272; (h) A. Yella, C.-L. Mai, S. M. Zakeeruddin, S.-N. Chang, C.-H. Hsieh, C.-Y. Yeh and M. Grätzel, *Angew. Chem. Int. Ed.*, 2014, **53**, 2973-2977.
3. S. Mathew, A. Yella, P. Gao, R. Humphry-Baker, F. E. CurchodBasile, N. Ashari-Astani, I. Tavernelli, U. Rothlisberger, K. NazeeruddinMd and M. Grätzel, *Nat. Chem*, 2014, **6**, 242-247.
4. (a) A. Mishra, M. K. R. Fischer and P. Bauerle, *Angew. Chem. Int. Ed.*, 2009, **48**, 2474-2499; (b) Y. Ooyama and Y. Harima, *Eur. J. Org. Chem.,* 2009, **2009**, 2903-2934; (c) X. Lu, Q. Feng, T. Lan, G. Zhou and Z.-S. Wang, *Chem. Mater.,* 2012, **24**, 3179-3187; (d) M. Liang and J. Chen, *Chem. Soc. Rev.,* 2013, **42**, 3453-3488; (e) Z. Wu, Z. An, X. Chen and P. Chen, *Org. Lett.*, 2013, **15**, 1456-1459; (f) N. Cai, J. Zhang, M. Xu, M. Zhang and P. Wang, *Adv. Funct. Mater.,* 2013, **23**, 3539-3547.
5. (a) N. Zhou, K. Prabakaran, B. Lee, S. H. Chang, B. Harutyunyan, P. Guo, M. R. Butler, A. Timalsina, M. J. Bedzyk, M. A. Ratner, S. Vegiraju, S. Yau, C.-G. Wu, R. P. H. Chang, A. Facchetti, M.-C. Chen and T. J. Marks, *J. Am. Chem. Soc.,* 2015, **137**, 4414-4423; (b) Y. Xie, Y. Tang, W. Wu, Y. Wang, J. Liu, X. Li, H. Tian and W.-H. Zhu, *J. Am. Chem. Soc.,* 2015, **137**, 14055-14058; (c) J. Yang, P. Ganesan, J. Teuscher, T. Moehl, Y. J. Kim, C. Yi, P. Comte, K. Pei, T. W. Holcombe, M. K. Nazeeruddin, J. Hua, S. M. Zakeeruddin, H. Tian and M. Grätzel, *J. Am. Chem. Soc.,* 2014, **136**, 5722-5730.
6. Z. Yao, M. Zhang, H. Wu, L. Yang, R. Li and P. Wang, *J. Am. Chem. Soc.*, 2015, **137**, 3799-3802.
7. (a) P. Wang, S. M. Zakeeruddin, J. E. Moser, M. K. Nazeeruddin, T. Sekiguchi and M. Grätzel, *Nat. Mater*, 2003, **2**, 402-407; (b) H. Wang, X. Zhang, F. Gong, G. Zhou, Z.-S. Wang, *Adv. Mater.*, 2012, **24**, 121-124.
8. M. Grätzel, *J. Photochem. Photobiol. A,* 2004, **164**, 3-14.
9. (a) R. Mondal, N. Miyaki, H. A. Becerril, J. E. Norton, J. Parmer, A. C. Mayer, M. L. Tang, J.-L. Bredas, M. D. McGehee and Z. Bao, *Chem. Mater.,* 2009, **21**, 3618-3628; (b) H. Qin, L. Li, Y. Li, X. Peng, J. Peng, Y. Cao, N. Ismayil and W. Shi, *Eur. Polym. J.,* 2012, **48**, 2076-2084.
10. X. Lu, G. Zhou, H. Wang, Q. Feng and Z.-S. Wang, *Phys. Chem. Chem. Phys.,* 2012, **14**, 4802-4809.
11. (a) Y. Wu and W. Zhu, *Chem. Soc. Rev.*, 2013, **42**, 2039-2058; (b) Y. Wu, W.-H. Zhu, S. M. Zakeeruddin and M. Grätzel, *ACS Appl. Mater. Interfaces.,* 2015, **7**, 9307-9318; (c) W. Zhu, Y. Wu, S. Wang, W. Li, X. Li, J. Chen, Z.-S. Wang and H. Tian, *Adv. Funct. Mater.,* 2011, **21**, 756-763; (d) Y. Cui, Y. Wu, X. Lu, X. Zhang, G. Zhou, F. B. Miapeh, W. Zhu and Z.-S. Wang, *Chem. Mater.,* 2011, **23**, 4394-4401; (e) Y. Wu, X. Zhang, W. Li, Z.-S. Wang, H. Tian and W. Zhu, *Adv. Energy Mater.*, 2012, **2**, 149-156; (f) Y. Wu, M. Marszalek, S. M. Zakeeruddin, Q. Zhang, H. Tian, M. Grätzel and W. Zhu, *Energy Environ. Sci.* 2012, **5**, 8261-8272; (g) H. Li, T. M. Koh, A. Hagfeldt, M. Grätzel, S. G. Mhaisalkar and A. C. Grimsdale, *Chem. Commun*, 2013, **49**, 2409-2411; (h) W. Ying, J. Yang, M. Wielopolski, T. Moehl, J.-E. Moser, P. Comte, J. Hua, S. M. Zakeeruddin, H. Tian and M. Grätzel, *Chemical Science*, 2014, **5**, 206-214.
12. (a) K. Pei, Y. Wu, H. Li, Z. Geng, H. Tian and W.-H. Zhu, *ACS Appl. Mater. Interfaces,* 2015, **7**, 5296-5304; (b) L.-P. Zhang, K.-J. Jiang, G. Li, Q.-Q. Zhang and L.-M. Yang, *J. Mater. Chem. A,* 2014, **2**, 14852-14857; (c) T. Lan, X. Lu, L. Zhang, Y. Chen, G. Zhou and Z.-S. Wang, *J. Mater. Chem. A,* 2015, **3**, 9869-9881; (d) Y. Xie, W. Wu, H. Zhu, J. Liu, W. Zhang, H. Tian and W.-H. Zhu, *Chem. Sci.*, 2016, **7**, 544-549.
13. (a) S. Qu, W. Wu, J. Hua, C. Kong, Y. Long and H. Tian, *J. Phys. Chem. C,* 2010, **114**, 1343-1349; (b) S. Haid, M. Marszalek, A. Mishra, M. Wielopolski, J. Teuscher, J. E. Moser, R. Humphry-Baker, S. M. Zakeeruddin, M. Grätzel and P. Bauerle, *Adv.*

Funct. Mater., 2012, **22**, 1291-1302; (c) J.-H. Yum, T. W. Holcombe, Y. Kim, J. Yoon, K. Rakstys, M. K. Nazeeruddin and M. Grätzel, *Chem. Commun*, 2012, **48**, 10727-10729; (d) S.-G. Li, K.-J. Jiang, J.-H. Huang, L.-M. Yang and Y.-L. Song, *Chem. Commun*, 2014, **50**, 4309-4311.

14. N. I. Abdo, A. A. El-Shehawy, A. A. El-Barbary and J.-S. Lee, *Eur. J. Org. Chem.,* 2012, **2012**, 5540-5551.
15. N. Miyaura and A. Suzuki, *Chem. Rev.,* 1995, **95**, 2457-2483.
16. M. Banno, T. Yamaguchi, K. Nagai, C. Kaiser, S. Hecht and E. Yashima, *J. Am. Chem. Soc.,* 2012, **134**, 8718-8728
17. E. Knoevenagel, *Justus Liebigs Ann. Chem.,*1894, **281**, 25-126.
18. A. F. Moretto, S. J. Kirincich, W. X. Xu, M. J. Smith, Z. K. Wan, D. P. Wilson, B. C. Follows, E. Binnun, D. Joseph-McCarthy, K. Foreman, D. V. Erbe, Y. L. Zhang, S. K. Tam, S. Y. Tam and J. Lee, *Bioorg. Med. Chem.*, 2006, **14**, 2162-2177.
19. (a) Y. Hong, J.-Y. Liao, D. Cao, X. Zang, D.-B. Kuang, L. Wang, H. Meier and C.-Y. Su, *J. Org. Chem.,* 2011, **76**, 8015-8021; (b) Y. Hao, X. Yang, M. Zhou, J. Cong, X. Wang, A. Hagfeldt and L. Sun, ChemSusChem, 2011, **4**, 1601-1605; (c) S. Haid, M. Marszalek, A. Mishra, M. Wielopolski, J. Teuscher, J.-E. Moser, R. Humphry-Baker, S. M. Zakeeruddin, M. Grätzel and P. Bäuerle, *Adv. Funct. Mater.,* 2012, **22**, 1291-1302.
20. A. Hagfeldt and M. Grätzel, *Chem. Rev.,* 1995, **95**, 49-68.
21. J.-L. Bredas, *Mater. Horiz,* 2014, **1**, 17-19.
22. A. Hagfeldt, G. Boschloo, L. Sun, L. Kloo and H. Pettersson, *Chem. Rev.,* 2010, **110**, 6595-6663.
23. M. J. Frisch, G. W. Trucks, H. B. Schlegel, G. E. Scuseria, M. A. Robb, J. R. Cheeseman, J. A. Montgomery, T. Vreven, K. N. Kudin, J. C. Burant, J. M. Millam, S. S. Iyengar,J. Tomasi, V. Barone, B. Mennucci, M. Cossi, G. Scalmani,N. Rega, G. A. Petersson, H. Nakatsuji, M. Hada, M. Ehara,K. Toyota, R. Fukuda, J. Hasegawa, M. Ishida, T. Nakajima,Y. Honda, O. Kitao, H. Nakai, M. Klene, X. Li, J. E. Knox,H. P. Hratchian, J. B. Cross, V. Bakken, C. Adamo, J. Jaramillo, R. Gomperts, R. E. Stratmann, O. Yazyev, A. J. Austin, R. Cammi, C. Pomelli, J. W. Ochterski, P. Y. Ayala, K. Morokuma, G. A. Voth, P. Salvador, J. J. Dannenberg, V. G. Zakrzewski, S. Dapprich, A. D. Daniels, M. C. Strain, O. Farkas, D. K. Malick, A. D. Rabuck, K. Raghavachari, J. B. Foresman, J. V. Ortiz, Q. Cui, A. G. Baboul, S. Clifford, J. Cioslowski, B. B. Stefanov, G. Liu, A. Liashenko, P. Piskorz, I. Komaromi, R. L. Martin, D. J. Fox, T. Keith, M. A. AlLaham, C. Y. Peng, A. Nanayakkara, M. Challacombe,P. M. W. Gill, B. Johnson, W. Chen, M. W. Wong,C. Gonzalez, J. A. Pople, Gaussian 03, Revision C.02, Gaussian, Inc., Wallingford, CT, 2004.
24. J. Luo, M. Xu; R. Li, K.-W. Huang, C.Jiang, Q. Qi, W. Zeng; J. Zhang, C. Chi, P. Wang and J. Wu, *J. Am. Chem. Soc.*, 2014, **136**, 265.
25. (a) K. Hara, Y. Dan-oh, C. Kasada, Y. Ohga, A. Shinpo, S. Suga, K. Sayama and H. Arakawa, *Langmuir*, 2004, **20**, 4205-4210; (b) K. Hara, T. Sato, R. Katoh, A. Furube, Y. Ohga, A. Shinpo, S. Suga, K. Sayama, H. Sugihara and H. Arakawa, *J. Phys. Chem. B,* 2003, **107**, 597-606; (c) H. Ozawa, R. Shimizu and H. Arakawa, *RSC Adv.,* 2012, **2**, 3198-3200.
26. K. Pei, Y. Wu, A. Islam, Q. Zhang, L. Han, H. Tian and W. Zhu, *ACS Appl. Mater. Interfaces,* 2013, **5**, 4986-4995.
27. Y. Chiba, A. Islam, R. Komiya, N. Koide and L. Han, *Appl.Phys. Lett.*, 2006, **88**, 223505.
28. G. Dennler, M. C. Scharber, and C. J. Brabec, *Adv. Mater.* 2009, **21**, 1 – 16.
29. T. Marinado, K. Nonomura, J. Nissfolk, M. K. Karlsson, D. P. Hagberg, L. C. Sun, S. Mori, and A. Hagfeldt, *Langmuir* 2010, **26**, 2592 – 2598.
30. (a) N. W. Duffy, L. M. Peter, R. M. G. Rajapakse and K. G. U. Wijayantha, *Electrochem. Commun.*, 2000, **2**, 658-662; (b) M. Bailes, P. J. Cameron, K. Lobato and L. M. Peter, *J. Phys.Chem. B*, 2005, **109**, 15429-15435.
31. (a) T. Oekermann, D. Zhang, T. Yoshida and H. Minoura, *J. Phys. Chem. B*, 2004, **108**, 2227-2235; (b) P.-T. Hsiao, Y.-L. Tung and H. Teng, *J. Phys. Chem. C*, 2010, **114**, 6762-6769.
32. (a) M. Miyashita, K. Sunahara, T. Nishikawa, Y. Uemura, N. Koumura, K. Hara, A. Mori, T. Abe, E. Suzuki and S. Mori, *J. Am. Chem. Soc.,* 2008, **130**, 17874-17881; (b) B. C. O'Regan, K. Walley, M. Juozapavicius, A. Anderson, F. Matar, T. Ghaddar, S. M. Zakeeruddin, C. Klein and J. R. Durrant, *J. Am. Chem. Soc.*, 2009, **131**, 3541-3548.
33. G. Schlichthörl, S. Y. Huang, J. Sprague and A. J. Frank, *J. Phys. Chem. B*, 1997, **101**, 8141-8155.
34. X. Ren, Q. Feng, G. Zhou, C.-H. Huang and Z.-S. Wang, *J. Phys. Chem. C*, 2010, **114**, 7190-7195.
35. (a) Z. Yu, D. Qin, Y. Zhang, H. Sun, Y. Luo, Q. Meng and D. Li, *Energy Environ. Sci.,* 2011, **4**, 1298-1305; (b) J.-J. Kim, H. Choi, J.-W. Lee, M.-S. Kang, K. Song, S. O. Kang and J. Ko, *J. Mater. Chem.*, 2008, **18**, 5223-5229; (c) S.-H. Park, I. Y. Song, J. Lim, Y. S. Kwon, J. Choi, S. Song, J.-R. Lee and T. Park, *Energy Environ. Sci.,* 2013, **6**, 1559-1564; (d) S.-Y. Shen, R.-X. Dong, P.-T. Shih, V. Ramamurthy, J.-J. Lin and K.-C. Ho, *ACS Appl. Mater. Interfaces*, 2014, **6**, 18489-18496.

Table of Contents Entry

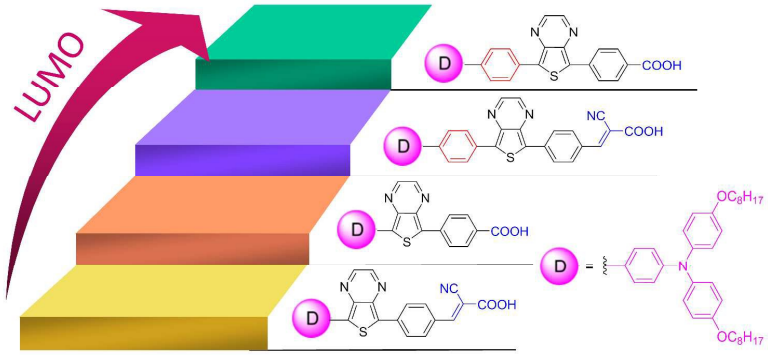

Energy levels of thieno[3,4-*b*]pyrazine based organic sensitizers have been successfully optimized for efficient quasi-solid-state dye-sensitized solar cells.